Chemical Engineering Journal 417 (2021) 127947

Contents lists available at ScienceDirect

Chemical Engineering Journal

journal homepage: www.elsevier.com/locate/cej

Engineering Janus CNTs/OCS composite membrane at air/water interface for excellent dye molecules screening

Tianyu Chen [a,b], Junyuan Xia [a], Jincui Gu [a,c,*], Guangming Lu [a], Qunji Xue [a], Chaohui Liu [d], Luke Yan [d,*], Tao Chen [a,c,d,*]

[a] Key Laboratory of Marine Materials and Related Technologies, Zhejiang Key Laboratory of Marine Materials and Protective Technologies, Ningbo Institute of Material Technology and Engineering, Chinese Academy of Science, Ningbo 315201, China
[b] Department of Nano Science and Technology Institute, University of Science and Technology of China, 166 Renai Road, Industrial Park, Suzhou, Jiangsu 215123, China
[c] School of Chemical Sciences, University of Chinese Academy of Science, Beijing 100049, China
[d] Polymer Materials & Engineering Department, School of Materials Science & Engineering, Chang' an University, Xi'an 710064, China

ARTICLE INFO

Keywords:
Janus membrane
Interpenetrating network
Asymmetric wettability
Molecular screening
Ultrahigh permeation

ABSTRACT

Two-dimensional (2D) membrane with ultrahigh permeability and precise sieving performance is highly desired. Herein, we have constructed a Janus composite membrane, which is integrated with carbon nanotubes (CNTs) and oxidized carbon spheres (OCS) modified with polyetherimide (PEI), through an interfacial self-assembly process. The designed Janus CNTs/OCS@PEI composite membrane has asymmetric micromorphology and wettability. The hydrophobic side is functioned as an active layer to inhibit concentration polarization during separation process. The superhydrophilic side can allow partial CNTs to stretch into its interior and form an interpenetrating network, which can weaken the Laplace pressure arising from the hydrophobic side. Hence, this membrane has the ability to reject various dye molecules, such as congo red (permeance flux of 3110.2 ± 285 L $m^{-2}h^{-1}$ bar^{-1} and efficiency about 98.8%), which has transcended the majority of the separation membranes previously reported. Furthermore, this membrane can withstand physical damage and chemical corrosion that has presented stable rejection performance for dye molecules. This intriguing work would open the door to developing novel Janus materials to satisfy the water resources requirements of real-world applications.

1. Introduction

Water is a natural resource essential for life. The purification of waste water containing dyes is one of the most urgent tasks that are closely related to ecosystem [1]. Currently, the removal of dye molecules is mainly through adsorption, catalytic degradation and membrane filtration [2]. Among these strategies, membrane separation technology is the most effective means to obtain sustainable water resource because it is environmentally benign and low energy consumption [3–4]. Recently, as representative separation membranes, such as graphene oxide (GO) [4–10], molybdenum disulfide (MoS_2) nanosheets [11–14], covalent organic framework (COF) nanosheets [15–17], metal–organic framework (MOF) nanosheets [18–20], Mxene [21–22] and g-C_3N_4 [23–24], have attracted increasing attention. These membranes endow with advantages of adjustable microstructure, stable chemical property and precise sieving ability [25,26]. Therefore, scientists have contributed considerable efforts and numerous exciting breakthroughs have sprung up. For example, Cao et al. [11] fabricated a MoS_2 membrane through vacuum filtration. It displayed excellent rejection ability (>90%) for various dye molecules (size >1.9 nm). Zeng et al. [20] have reported an UiO-66 TFC membrane through polydopamine modification and then phase immersion conversion. It showed high rejection ability for various dye molecules. Chen et al. [27] have presented a graphene-based membrane with large scale through a self-assembly process. This membrane displayed an excellent screening capacity (>98%) for dye molecules and the flux reached up to 191 L $m^{-2}h^{-1}$ bar^{-1}. Although remarkable progress has been achieved, the current bottleneck remains the "trade-off "between permeation and rejection. On the one hand, a higher flux is usually achieved by decreasing membrane dimension or broadening aperture size. However, the rejection performance is compromised to a certain degree [28–29]. On the other hand, the permeation flux is critically sacrificed because of increasing hydraulic

* Corresponding authors.
E-mail addresses: gujincui@nimte.ac.cn (J. Gu), tao.chen@nimte.ac.cn (T. Chen).

https://doi.org/10.1016/j.cej.2020.127947
Received 23 August 2020; Received in revised form 27 October 2020; Accepted 27 November 2020
Available online 3 December 2020

resistance, which is arisen from the internal concentration polarization across these isotropic interfaces [30–32].

Janus interfaces endow materials with novel physical and chemical properties, which take on irreplaceable roles in broad fields. To date, researchers have constructed a series of Janus membranes to settle the intractable issues encountered in various separations [33–36]. For example, Jiang et al. have developed a Janus membrane by patterning polymer clusters onto GO surface [36]. By coupling the advantages of polymer clusters and interlayer channels, this membrane presented an excellent nanofiltration performance for polar or non-polar solvents. Chung et al. have constructed a Janus film via an interfacial polymerization between cyclodextrin and trimesoyl chloride [37]. The hydrophobic inner cavities have facilitated the transfer of nonpolar solvents, and whereas the hydrophilic interface has provided an expressway for polar solvents. Wang et al. [38] have displayed a Janus membrane which exhibited high rejection capacity (>95%) for dye molecules. Liu et al. [32] have contracted a Janus membrane which was comprised with superhydrophobic silica and superhydrophilic polyvinylidene fluoride. This membrane presented an excellent separation performance for dye molecules under the joint effect of hydrophilic side and hydrophobic side. Despite these pioneering works, the preparation methods of these membranes are spin-casting, drop-casting, spraying and vacuum filtration [39]. Moreover, they are restricted by abundant organic solvents and relatively low permeability flux [40]. Therefore, it is urgently expected to develop an advanced Janus membrane for superior screening performance through an ultrafast and environmentally friendly strategy.

In previous work, we have prepared a series of membranes through an interfacial self-assembly process at ail/water surface and subsequent asymmetric modification [41,42]. The wettability can be controlled by adjusting the hydrophobic/hydrophilic groups of polymers. Moreover, this strategy does not need expensive instruments. By virtue of these merits, we here firstly presented a Janus carbon-based membrane by combining hydrophobic carbon nanotubes (CNTs) and hydrophilic oxidized carbon spheres (OCS) nanoparticles modified with polyetherimide (PEI). The smooth inner wall of CNTs has low mass transfer resistance, which can increase separation flux [43]. Moreover, it possesses with high surface area that is beneficial to achieve effective adsorption with dye molecules [44]. PEI is provided with rich amino groups that make it possible to react with OCS through chemical crosslinking or hydrogen bonding [45]. The obtained membrane has abundant micro-nano apertures and Janus wettability with the hydrophilic/hydrophobic discrepancy attaining to 110°. Moreover, the hydrophobic side is acted as a repelling layer to minimize concentration polarization. The hydrophilic side can permit partial CNTs to stretch into its interior and form an interpenetrating network for decreasing Laplace pressure. Under the joint effect of abundant porous geometry, anisotropic wettability and interpenetrating network, this Janus membrane presents ultrafast screening performance for dye molecules, such as congo red (with the permeance coming up to 3110.2 ± 285 L $m^{-2}h^{-1}$ bar^{-1} and efficiency about 98.8%), which is superior to the majority of the separation membranes previously reported so far.

2. Experimental

2.1. Materials

CS powder (diameter: ~50 nm) was supplied by Nafortis Technology Co. Ltd (Shanghai, China) prepared by gas phase detonation. Carbon nanotubes (CNTs, purity > 97%, 10–30 μm length and 8–15 nm diameter, 0.45 wt% $–NH_2$) were offered from Chengdu Organic Chemistry Co., Ltd. Polyethyleneimine (PEI) (M_W: 600 g/mol–70,000 g/mol) were got from Aladdin (Shanghai) Co., Ltd. Noting: the concentration of PEI was 0.01 mg/mL. Nylon filter paper (average pore size 220 nm) was purchased from Healthcare Life Sciences. Different dye molecules, including methyl orange (MO, 1.2 nm × 0.7 nm, 327.33 g/mol), rhodamine B (RhB, 1.8 nm × 1.4 nm, 479.01 g/mol), victoria blue B (VBB, 1.5 nm × 2.0 nm, 506.08 g/mol), acid fuchsin (AF, 1.0 nm × 1.0 nm, 585.54 g/mol), congo red (CR, 1.3 nm × 2.8 nm, 696.68 g/mol), methyl blue (MB, 1.9 nm × 2.5 nm, 799.80 g/mol), evans blue (EB, 3.1 nm × 1.3 nm, 960.81 g/mol), acid red 94 (AR, 1.2 nm × 1.5 nm, 1017.64 g/mol), alcian blue 8 (AB, 2.3 nm × 2.3 nm, 1298.86 g/mol) were purchased from Sigma-Aldrich Co., Ltd. Anhydrous ethanol and water were used as rinsing solvents.

2.2. Preparation of the CNTs membrane

Firstly, 120 mL of CNTs ethanol dispersion (0.2 mg/mL, pH = 7.0) was sprayed onto the air/water interface (pH = 7.0). Secondly, a porous sponge was put on one side to compress the CNTs layer. Lastly, the CNTs layer was parallelly transferred to the hydrophilic nylon substrate and further dried under 60 °C for 4 h to get the CNTs membrane. The comparison of the preparation process of various membranes was shown in Table S1.

2.3. Preparation of CNTs@PEI composite membrane and OCS@PEI composite membrane

Firstly, CS powder was oxidized with hydrogen peroxide for 4 days under 45 °C. Secondly, they were cleaned with distilled water and anhydrous ethanol alternately for three times and dried in a vacuum oven at room temperature for 4 h. Thirdly, the CNTs ethanol dispersion (0.2 mg/mL, 120 mL, pH = 7.0) or OCS ethanol dispersion (0.2 mg/mL, 120 mL, pH = 7.0) were sprayed onto the air/PEI solution interface (pH = 7.0), respectively. Thirdly, a porous sponge was applied for compressing the CNTs@PEI layer or OCS@PEI layer. Lastly, they were parallelly transferred to the hydrophilic nylon substrate and dried under 60 °C for 4 h to obtain the responding CNTs@PEI composite membrane and OCS@PEI composite membrane.

2.4. Preparation of the CNTs/OCS@PEI composite membrane with a mixed structure

Firstly, 80 mL of CNTs ethanol dispersion (0.2 mg/mL, pH = 7.0), 40 mL of OCS ethanol dispersion (0.2 mg/mL, pH = 7.0) were mixed by ultrasonication for 1 h to form a homogeneous dispersion. Secondly, the dispersion was sprayed onto the air/PEI solution (pH = 7.0) interface. Thirdly, a porous sponge was put on one side to compress the CNTs/OCS@PEI layer. Lastly, the CNTs/OCS@PEI membrane was transferred to the hydrophilic nylon substrate and dried under 60 °C for 4 h to gain the CNTs/OCS@PEI composite membrane with a mixed structure (M-CNTs/OCS@PEI membrane).

2.5. Preparation of the CNTs/OCS@PEI composite membrane with double-layer structure

Firstly, 80 mL of CNTs ethanol dispersion (0.2 mg/mL, pH = 7.0), 40 mL of OCS ethanol dispersion (0.2 mg/mL, pH = 7.0) were sprayed onto the air/water interface or air/PEI solution (pH = 7.0) interface, respectively. Secondly, a sponge was employed to extrude the CNTs or OCS@PEI layer. Thirdly, a silicon wafer was used to transfer the CNTs layer onto OCS@PEI layer. Lastly, the CNTs/OCS@PEI layer was transferred to nylon substrate and then dried under 60 °C for 4 h to acquire the CNTs/OCS@PEI composite membrane with double-layer structure (D-CNTs/OCS@PEI membrane).

2.6. Preparation of the Janus CNTs/OCS@PEI membrane with interpenetrating network structure

Firstly, 40 mL of OCS ethanol dispersion (0.2 mg/mL, pH = 7.0) was successively sprayed onto the air/PEI solution (pH = 7.0) interface. Secondly, 80 mL of CNTs ethanol dispersion (0.2 mg/mL, pH = 7.0) was

sprayed onto the air/PEI solution (pH = 7.0) interface. During this process, some CNTs have embedded inside of the OCS@PEI layer. Thirdly, a porous sponge was put on one side to compress the CNTs/OCS@PEI layer. Lastly, the CNTs/OCS@PEI membrane was transferred to the hydrophilic nylon substrate and dried under 60 °C for 4 h to gain the Janus CNTs/OCS@PEI composite membrane with interpenetrating network structure.

2.7. Screening performance of each membrane

The permeation process was carried out on a cross-flow filtration system with an effective area about 6 cm^2. The permeance flux was evaluated after 1 h under a pressure of 1 bar.

The separation flux J was calculated according to the equation:

$$J = V/(S \times T) \quad (1)$$

where V (L) was the feed volume, S (m^2) was the filtration area, T (h) was the permeate time.

The separation efficiency (R) was calculated by the following equation:

$$R = \left(1 - C_p/C_o\right) \times 100\% \quad (2)$$

where C_o and C_p were the concentrations of the dye molecules in the feed and filtration.

2.8. Characterization

The microstructure of each sample was carried on the scanning electronic microscopy (SEM, Hitachi S4800, Japan), transmission electronic microscopy (TEM, JEOL2100 HR, America) and Focused Ion Beam (FIB, Helios-G4-CX, America). Each membrane was tested for three times to acquire its accurate topography. The pore size distribution of each membrane was obtained from SEM image. The wettability was carried out on the contact angle measuring instrument (OCA-100, America) at the room temperature with 3 μL water droplet on the membrane surface. Five different positions were measured for each sample. The specific surface area was tested on the automated gas sorption analyzer (ASAP2020HD88, America) under N_2 environment for 12 h. The chemical composition was analyzed on the X-ray photoelectron spectroscopy (XPS, Axis Ultra DLD, Kratos, Japan). To quantify the thicknesses of individual layers in the membrane, the element composition was analyzed with a step length of 20 nm from the membrane surface to interior with depth up to 200 nm. The zeta potential of each membrane was measured on the zeta potential analyzer (Nano ZS, SurPASS 3, England). Each membrane was tested for three times to get the average value. The concentration of each dye molecular was analyzed by the UV–visible spectrophotometer (UV–vis, Lambda 950, Germany). Each result was measured for three times to obtain an accurate result.

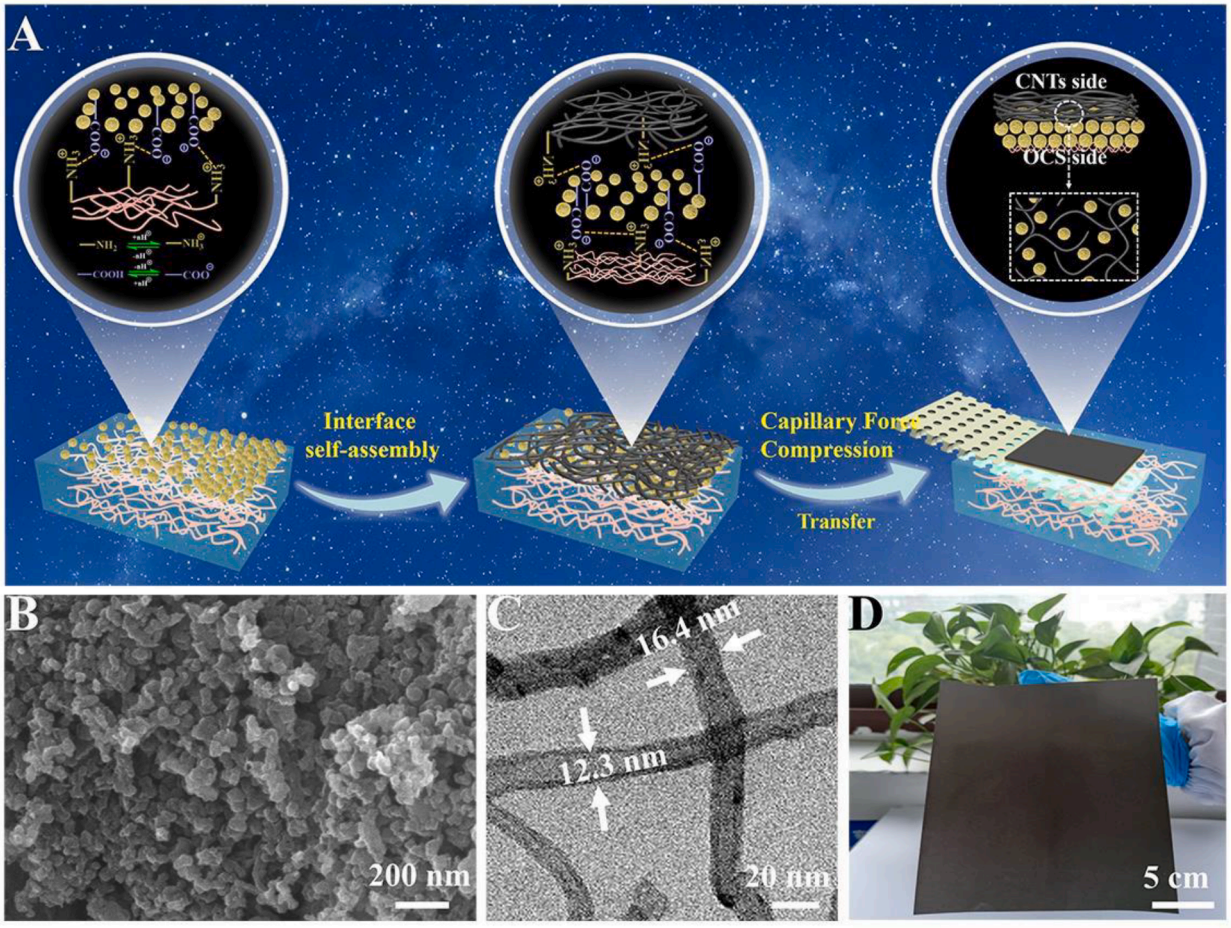

Fig. 1. (A) Schematic description of the preparation process of the Janus CNTs/OCS@PEI composite membrane at the air/water interface. Firstly, the OCS dispersion was sprayed onto the air/PEI solution surface evenly. The electrostatic force between OCS and PEI can facilitate the formation of hydrophilic OCS@PEI layer at air/water surface. Secondly, the CNTs ethanol dispersion was subsequently spayed on the OCS@PEI layer. During this process, partial CNTs can insert the inner of the OCS@PEI layer. Lastly, the Janus CNTs/OCS@PEI composite membrane was shifted onto the nylon substance after being compressed with a porous sponge. (B) The SEM image of the CS particles. (C) The TEM image of the CNTs. (D) Photograph of the Janus CNTs/OCS@PEI composite membrane with large scale.

3. Results and discussion

3.1. Janus structure and chemical composite

The architecture of the Janus CNTs/OCS@PEI composite membrane was illustrated in Fig. 1A and Fig. S1. Firstly, the OCS ethanol dispersion was sprayed onto the air/PEI solution interface. Due to the strong Marangoni force, the OCS rapidly spread from the ethanol-rich areas with lower surface tension to the water-rich areas with higher surface tension. The positive/negative charge force between OCS and PEI was beneficial to form the OCS@PEI layer on air/water interface. Secondly, the CNTs dispersion was uniformly sprayed onto the OCS@PEI interface to form a CNTs/OCS@PEI layer. Then, a porous sponge was put on one side of the air/water surface and compressed the layer from a loosely to a closely state. Lastly, the CNTs/OCS@PEI membrane was shifted to a porous nylon substance (Fig. S2).

The microstructure of the CS nanoparticles before and after being oxidized was firstly surveyed by SEM and TEM. As shown in Fig. 1B, Fig. S3-S4, the CS nanoparticle (diameter of 52 ± 4 nm) presented a spherical shape with some irregular folds on its surface. After being oxidized with hydrogen peroxide, its specific surface area increased from 107 m^2/g to144 m^2/g (Fig. S5), which can promote its dispersion in ethanol solution (Fig. S3). The morphology of CNTs was also surveyed by SEM. The mean diameter of CNTs was 14 nm (Fig. 1C, Fig. S6). They tangled with each other and formed a non-aggregation network structure (Fig. S7). During the self-assembly process, they uniformly spread on the OCS@PEI layer. After being transferred to the porous nylon substrate, a CNTs/OCS@PEI composite membrane with a Janus structure was obtained (Fig. 1D, Fig. S8). The morphology of the Janus CNTs/OCS@PEI composite membrane was surveyed by SEM and FIB. The top side of this Janus membrane was the randomly distributed CNTs network with an average thickness of about 254 ± 22 nm (Fig. 2A-2B, Fig. S9). The bottom side of this membrane was the dense OCS nanoparticles with the average cross-sectional dimension of 135 ± 15 nm (Fig. 2C-2D, Fig. S9). Furthermore, the CNTs/OCS@PEI composite membrane showed different pore size distribution. The CNTs side has a larger pore size distribution that of the OCS@PEI side (Fig. 2E).

Besides, the Janus CNTs/OCS@PEI composite membrane possessed with anisotropic wettability. As shown in Fig. 2F, Movies S1 and S3, there was a little change of the CNTs side between CNTs membrane (135 ± 6.0°) and Janus CNTs/OCS@PEI composite membrane (115 ± 3.5°). However, the wettability of the OCS side was reduced from hydrophilicity (73 ± 2.0°) to superhydrophilicity (1 ± 1.0°) after the modification of PEI (Movies S2 and S4). This asymmetric wettability will be benefit for the transport of water from the hydrophobic to hydrophilic side [46–47]. It was noteworthy that this Janus membrane has a special interpenetrating network, which was critically important for water penetration performance (Fig. 2G, Fig. 2H). Furthermore, they were tightly interconnected with each other and the thickness of this Janus membrane was 347 ± 28 nm (Fig. 2I, Fig. S9).

The pore size distribution of the CNTs/OCS membrane and the Janus membrane was further investigated. The Janus CNTs/OCS@PEI membrane has a uniform aperture with the average size of 500 nm (Fig. 3A), which was smaller than that of the CNTs/OCS membrane (Fig. 3B). This

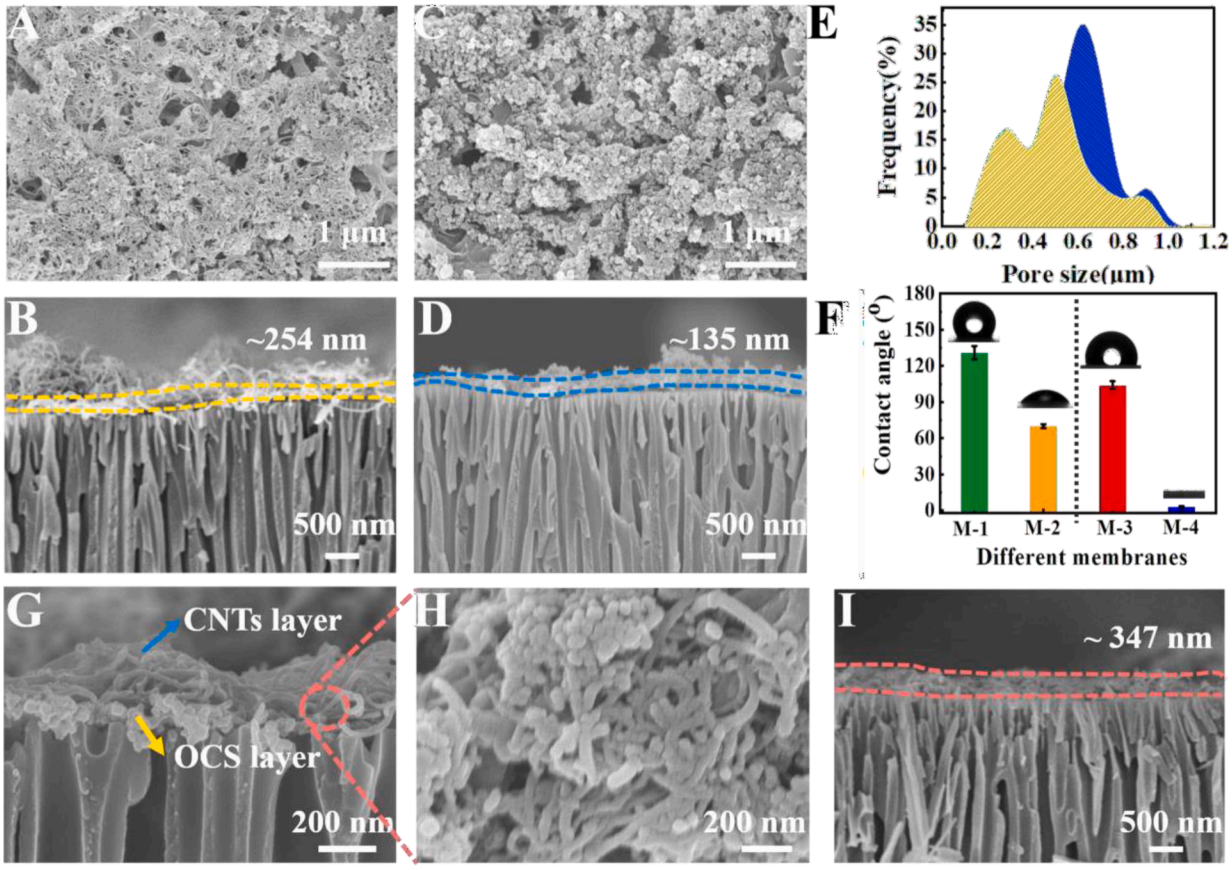

Fig. 2. SEM images of (A) the CNTs layer and (C) OCS layer of the Janus CNTs/OCS@PEI membrane, respectively. FIB results of the cross-sectional images of (B) CNTs membrane and (D) OCS@PEI membrane, respectively. (E) The pore size distribution of the CNTs side (blue) and the OCS (yellow) side of the Janus CNTs/OCS@PEI membrane, respectively. (F) The wettability of the CNTs membrane (M-1), OCS membrane (M-2), the CNTs side (M-3) and the OCS side (M-4) of the Janus CNTs/OCS@PEI composite membrane, respectively. (G) The SEM image of the cross-section of the Janus CNTs/OCS@PEI membrane and (H) its magnified SEM image of the interpenetrating structure. (I) The FIB result of the cross-sectional image of the Janus CNTs/OCS@PEI membrane. (For interpretation of the references to colour in this figure legend, the reader is referred to the web version of this article.)

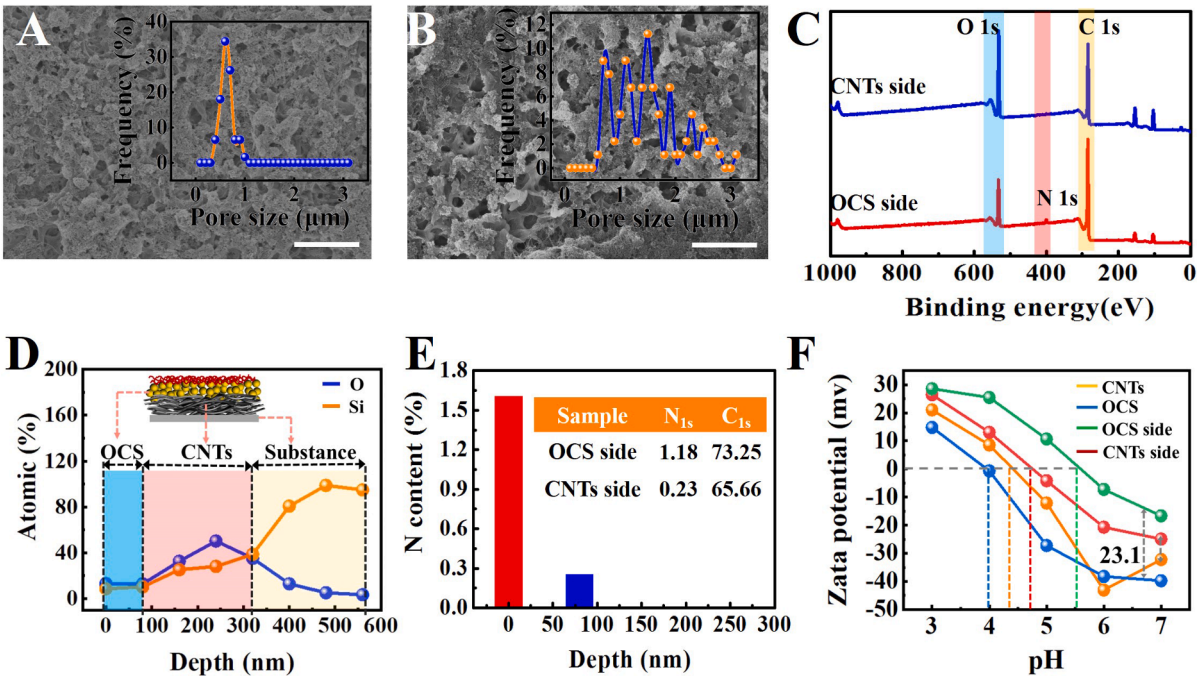

Fig. 3. The SEM image of the (A) Janus CNTs/OCS@PEI membrane and (B) CNTs/OCS membrane (Insert: their responding aperture size distribution). (C) The XPS spectrum of the CNTs and the OCS side of the Janus CNTs/OCS@PEI membrane, respectively. (D) XPS depth analysis results of the Janus CNTs/OCS@PEI membrane. (E) The change of N element content in the Janus CNTs/OCS@PEI membrane during the XPS etching process (Insert: the XPS result of the contents of N element and C element in both side of the Janus CNTs/OCS@PEI membrane). (F) The zeta potential of each membrane (including CNTs membrane, OCS membrane, the CNTs and the OCS side of the Janus CNTs/OCS@PEI membrane) in different pH environments, respectively.

indicated that PEI was assumed the role of a bridge to make discrete OCS nanoparticles packed tightly [48]. XPS measurements were also performed to test the chemical composition of this membrane. C 1s (298 eV) and O 1s (540 eV) peaks were presented for both sides of the Janus CNTs/OCS@PEI composite membranes (Fig. 3C). However, N 1s (at 402 eV) was only observed on the OCS side of this membrane, but not appeared on the CNTs side despite of a low content of amino groups in CNTs. Furthermore, XPS depth analysis was carried out to differentiate the O element in the CNTs/OCS@PEI composite membrane (from the OCS side to the CNTs side) and Si elements (from the wafer substrate) with the change of depth. As shown in Fig. 3D, the content of O element increased in the etching process. However, the content of N element was gradually decreased (Fig. 3E). These results were consistent with the element contents of this Janus membrane (Fig. 3E). In addition, the zeta potential of the CNTs and OCS sides of the Janus membrane were different from that of the pristine CNTs membrane and OCS membrane (Fig. 3F), respectively. On the one hand, the isoelectric point of OCS side after being modified with PEI has increased from 4.0 to 5.6, and whereas the isoelectric point of the CNTs side has only changed from 4.3 to 4.6. On the other hand, in the case of neutral solution (pH = 7), the zeta potential difference between the OCS side of Janus membrane (−16.6 ± 1.15 mV) and the pristine OCS membrane (−39.7 ± 0.23 mV) was higher than that of the CNTs side (−24.9 ± 2.36 mV) and the CNTs membrane (−34.2 ± 0.42 mV). These results demonstrated that the CNTs/OCS@PEI composite membrane has displayed Janus chemical composition after being modified with PEI.

3.2. Membrane screening property

In order to explore screening performance of the Janus CNTs/OCS@PEI composite membrane, a laboratory cross-flow filtration device was built (Fig. S10). Different dye molecules, including cationic dye molecules (RhB, VBB, AB) and anionic dye molecules (MO, AF, CR, MB, EB, AR) with different charges, sizes and molecular weights, were used to assess its separation performance (Fig. S11, Table S2). The initial concentration of these dye molecules was 50 mg/L. A series of comparative experiments were carried out to achieve an advanced membrane with excellent rejection performance. Firstly, the Janus membranes with different mass ratios (CNTs/OCS: 1/3, 1/2, 1/1, 2/1, 3/1) were fabricated for separating dye molecules. The Janus CNTs/OCS@PEI membrane showed excellent rejection efficiency for EB (~99.89%) when the mass ratio of CNTs and OCS was 2:1 (Fig. S12A). Excessive CNTs or OCS may bring about agglomeration, which resulted in low retention capacity. Secondly, we investigated the influence of the molecular weight of PEI on the separation performance of the Janus membrane. Its rejection performance has achieved the maximum when the molecular weight of PEI was 1800 g/mol (Fig. S12B-12C). The lower molecular weight (600 g/mol) endowed this membrane with a relatively weak degree of crosslinking. However, the higher molecular weights (10,000 g/mol and 70,000 g/mol) brought about excessive steric hindrance and caused a sharp decline of rejection [49]. Besides, systematic comparison experiments were implemented to evaluate the dye rejection performance of various membranes. As shown in Fig. 4**A** and **Table S3**, the Janus CNTs/OCS@PEI_{1800} membrane presented better retention performance than that of other membranes. On the one hand, the CNTs membrane, CNTs/OCS membrane and CNTs@PEI_{1800} membrane and M-CNTs/OCS@PEI_{1800} membrane with larger apertures and loose separation layer were not conducive to reject dye molecules (Fig. S13). Therefore, these membranes displayed lower separation efficiency for CR (70%–80%) and MB (60%–88%). On the other hand, the OCS@PEI_{1800} membrane with uniform wettability on both sides caused dye molecules to be accumulated on its hydrophilic surface (Fig. S14). This resulted in the concentration polarization in the inner and external of the separation layer and then brought about high resistance to water transport. As a consequence, the OCS@PEI_{1800} membrane has a lower separation throughput than that of the CNTs/OCS@PEI_{1800} membrane. With regard to the D-CNTs/OCS@PEI_{1800} membrane, it also presented low rejection performance for CR (52.8% ± 1.2%) and MB (60.9% ± 0.7%) due to its large aperture (Fig. S15). The above results further verified that CNTs networks stretched into the inner of the OCS@PEI_{1800}

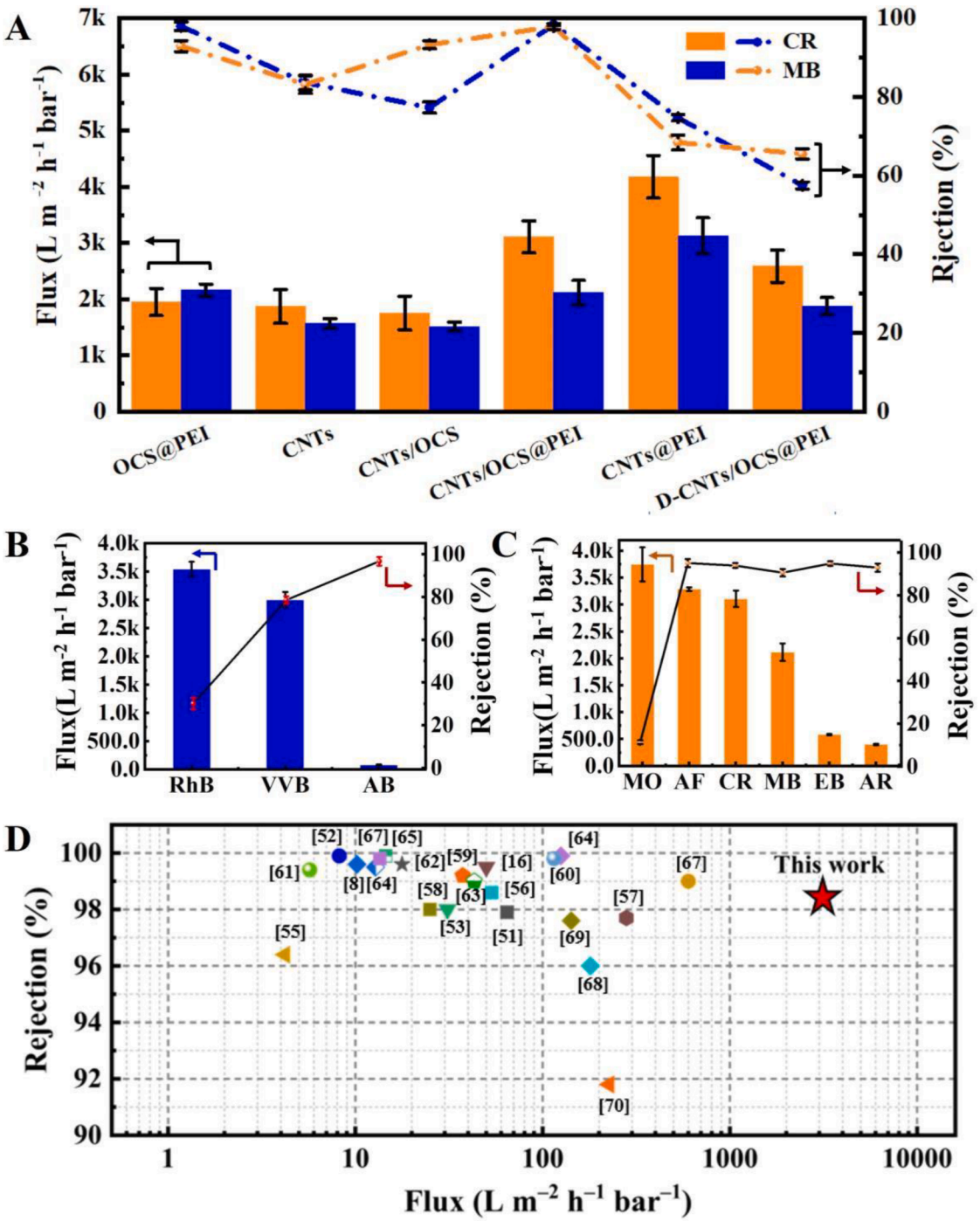

Fig. 4. (A) The separation performance of different membranes for CR and MB solutions, respectively. The rejection performance of the Janus CNTs/OCS@PEI$_{1800}$ membrane for (B) cationic dye molecules (RhB, VVB, AB) and (C) anionic dye molecules (MO, AF, CR, MB, EB, AR), respectively. (D) The comparison of different membranes previously reported and this work for the rejection performance of CR.

side, which was served as a nanofluidic pipeline for water transport.

The separation performance of the Janus CNTs/OCS@PEI$_{1800}$ composite membrane for various dye molecules was further explored to evaluate its potential for water purification. As shown in Fig. 4B, it presented excellent retention ability for VVB and AB with rejection efficiency of 88.6 ± 1.7% and 96.7 ± 2.0%, respectively. However, it has lower separation ability for RhB with efficiency of 20.1 ± 2.7% despite it displayed a higher separation flux (3542.5 ± 129 L m^{-2}h^{-1} bar^{-1}) (Fig. S16). Furthermore, this membrane displayed excellent screening performance for anionic dye molecules. As shown in Fig. 4C, the penetration flux of AF, CR, MB, EB, AR solutions were about 3288.71 ± 33.59 L m^{-2}h^{-1} bar^{-1}, 3110.2 ± 285 L m^{-2}h^{-1} bar^{-1}, 2117.91 ± 216 L m^{-2}h^{-1} bar^{-1}, 584 ± 114 L m^{-2}h^{-1} bar^{-1}, 390.67 ± 10.8 L m^{-2}h^{-1} bar^{-1}, respectively. In addition, it has shown excellent rejection capacity for these dye molecules with efficiency above 96.7%. However, the rejection of MO solution was only 12.0 ± 0.9% despite of a higher flux (3749.513 ± 317 L m^{-2}h^{-1} bar^{-1}) (Fig. S17). Therefore, this membrane can be used as the gate for separating anionic dye molecules with different sizes. It was noting that the permeability flux of CR solution reached up to 3110.2 ± 285 L m^{-2}h^{-1} bar^{-1}, which was far beyond most of the state-of-art membranes previously reported with similar rejection efficiency [51,53–70] (Fig. 4D, Table S4). The rejection mechanism of

this membrane was shown in Fig. S18. On the one hand, it was attributed to size screening [9,25]. The interconnected nanochannels between CNTs and OCS were the main permeation channel. According to the size sieving theory, a separation membrane can allow smaller particles to permeate through the membrane, and whereas components larger than its pore size are retained. Therefore, the Janus membrane can be used for the separation of various dye molecules with different molecular weights or sizes. On the other hand, the rejection of the dye molecules was due to Donnan balance [50]. As to cationic dye molecules, they were adsorbed on the Janus membrane interface due to the electrostatic force. Under this case, the concentration of cationic ion in the composite membrane was greater than that in the solution. Whereas, the concentration of the anionic ion of cationic dye molecules in the composite membrane was lower than that in the feed. The resulting Donnan position difference can prevent the diffusion of anionic ion the membrane surface in order to maintain electrical neutrality. However, with regard to anionic ion dyes molecules, they are rejected on the surface of the membrane surface because of the charge repulsion effect. Similarly, the cationic ions were rejected on the membrane surface in order to keep charge balance. Therefore, the rejection of the dye molecules of the Janus CNTs/OCS@PEI$_{1800}$ composite membrane was attributed to the collective effect of size screening and Donnan balance.

Interestingly, the Janus CNTs/OCS@PEI$_{1800}$ composite membrane has shown asymmetric separation flux for dye molecules with the same rejection. The hydrophobic CNTs side of this membrane has a higher permeability flux than that of the hydrophilic OCS@PEI$_{1800}$ side (Fig. S19), which was due to its Janus wettability and internal interpenetrating structure [46–47,71]. The physical stability of the Janus CNTs/OCS@PEI$_{1800}$ composite membrane was investigated. As shown in Fig. S20, the membrane kept its macro-morphology even after being bent for 12 times. It also showed excellent rejection performance for CR. In addition, the chemical stability of this membrane was tested after it was treated with harsh solutions for different times. As presented in Fig. S21, there was no change of the micro-topography of this membrane. Moreover, it also has stable separation flux and rejection ability for CR. These results demonstrated that the Janus CNTs/OCS@PEI$_{1800}$ composite membrane has excellent stability for further application.

3.3. Mechanism analysis

Water transport in the porous membranes is a complicated process. Several factors, such as hydrophobic pressure, surface roughness and chemical component, pore size distribution, etc., have played vital roles in water molecular penetration through membranes [72]. To illustrate the water transport process in the porous membrane, the aperture was simply modeled as the regular arrangement. Here, we described different cases of water penetration modes for different porous separation membranes. As to a fully hydrophobic CNTs membrane (Fig. 5A), the water molecule will be prevented from penetrating the interior of the membrane. That is because it has suffered from a contrary Laplace pressure (P_L), which is contrary to the hydraulic pressure (P_H) and the action pressure (P_A) direction [33,73]. For a given water droplet with a certain volume, P_H is a constant that is related to the height of the water droplet. The Laplace pressure can be evaluated by the following Young's equation:

$$p = \frac{2\gamma cos\theta}{r}$$

where, γ is the interface tension between gas and liquid; θ is the WCA of the membrane interface; r represents the membrane pore radius.

The difference of these pressures can be quantified as the following:

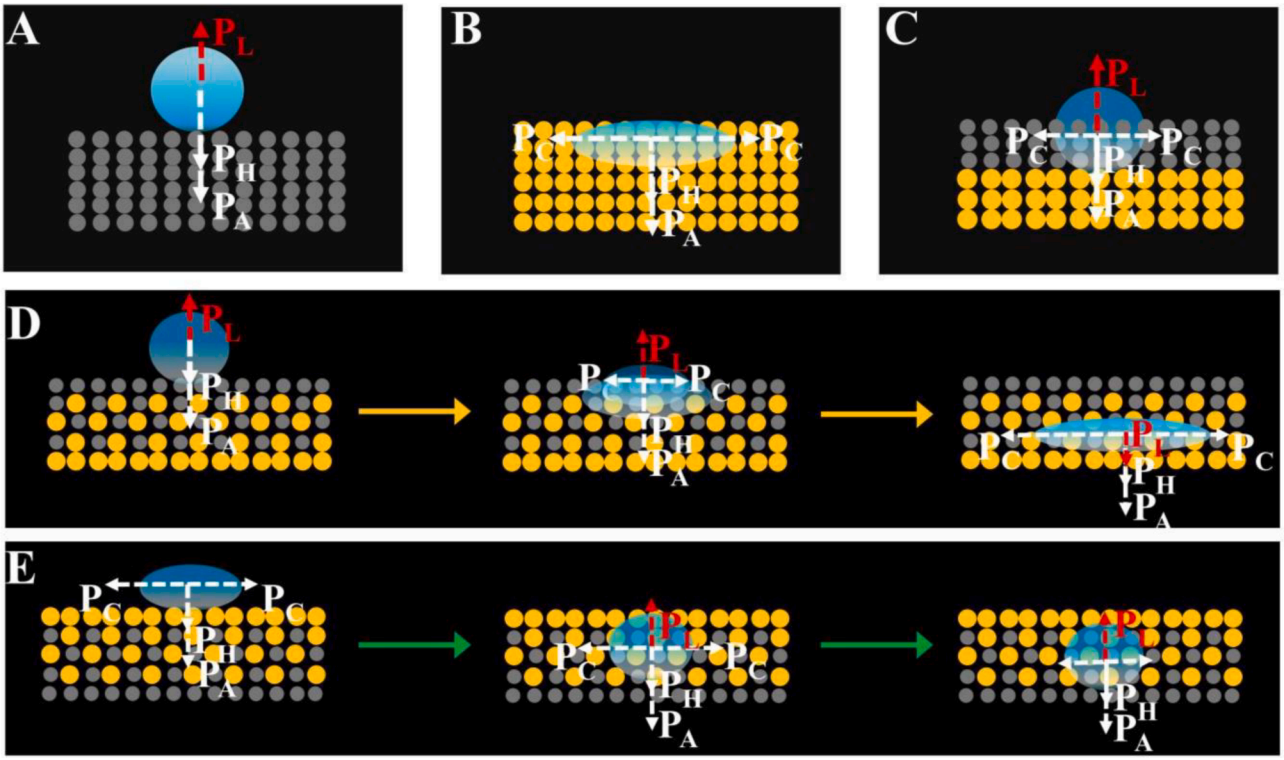

Fig. 5. Mechanism of water penetration performance on composite membranes with different wettability and microstructure. (A) The water droplet on an isotropic hydrophobic CNTs membrane was blocked arising from the Laplace pressure. (B) The water droplet could penetrate through the hydrophilic OCS@PEI$_{1800}$ membrane under the collective effect of hydraulic pressure, the action pressure, and capillary pressure. (C) The penetration behavior of the water droplet on a D-CNTs/OCS@PEI$_{1800}$ membrane. Laplace pressure is not conducive to the contact of water molecules with the hydrophilic layer. The penetration behavior of the water droplet on a Janus CNTs/OCS@PEI$_{1800}$ membrane with interpenetrating structure, (D) form the hydrophobic CNTs layer to the hydrophilic OCS@PEI$_{1800}$ layer (upper) and (E) from the hydrophilic OCS@PEI$_{1800}$ side to the hydrophobic CNTs side.

$$\Delta P = P_A + P_H - P_L + \rho gh - \frac{2\gamma cos\theta}{r}$$

Under the case of the sum of p_H and P_A exceeding the maximum P_L ($\Delta P > 0$), the water molecule can break through and penetrate the hydrophobic CNTs membrane. For the fully hydrophilic membrane, such as OCS@PEI_{1800} composite membrane (Fig. 5B), the water molecule can spontaneously infiltrate and pass through the membrane interface benefit from its capillary pressure (P_C) [47,74]. With regard to the anisotropic composite membranes, the water movement behavior is quite different from that of the isotropic counterparts. There are two circumstances for membranes with anisotropic wettability, which include forming the hydrophobic side to the hydrophilic side, and vice versa. Fig. 5C presented the water transport mechanism in the D-CNTs/OCS@PEI_{1800} composite membrane with an anisotropic structure. Owing to Laplace pressure, the water will form a meniscus on the hydrophobic CNTs side if there is nothing underneath. However, the hydrophilic OCS@PEI_{1800} layer will eliminate the Laplace pressure once the water meniscus is contacted with hydrophilic side due to the capillary force [32]. Therefore, the D-CNTs/OCS@PEI_{1800} composite membrane exhibited water penetration behavior. The above results indicated that there are two vital factors for achieving the excellent water molecular transport performance across the membrane [32,52]. One is that the Janus CNTs/OCS@PEI_{1800} membrane has opposite wettability of both sides. This has been demonstrated by the previously reported work [74,75]. The other is that the distance between the hydrophobic and the hydrophilic side ought to be as short as possible in order to reduce the Laplace pressure [52].

In this work, we designed a Janus CNTs/OCS@PEI_{1800} membrane, which the CNTs was partially inserted into the gaps of OCS@PEI_{1800} membrane. As far as the hydrophobic side was concerned, it can be seen that the curvature of the water meniscus as well as the P_L could be minimized in comparison with that of the traditional contact model attributing to its overlap interpenetrating microstructure (Fig. 5D). As soon as the water phase touched with the interpenetrating structure, the hydrophilic OCS@PEI_{1800} side was activated and the Laplace pressure promoted water to permeate through the whole membrane. In reverse, as to the Janus membrane from the OCS@PEI_{1800} layer (hydrophilic) to CNTs (hydrophobic) direction, the water droplet has a penetration model, which was similar to that of fully isotropic CNTs membrane (Fig. 5E). Laplace pressure from the hydrophobic CNTs side inhibited the rapid transport of water. Therefore, it showed lower water permeation.

4. Conclusions

In summary, an innovative Janus CNTs/OCS@PEI composite membrane was successfully prepared through an interfacial self-assembly process at the air/water interface. The obtained membrane possessed with substantial micro/nano pores, which can be acted as the transportation channels for water molecules. Importantly, it has taken on anisotropic wettability with the hydrophilic/hydrophobic difference beyond 110°. The hydrophobic CNTs side was used to minimize concentration polarization to a certain extent. Particularly, some CNTs networks can permit into the inner of the hydrophilic OCS@PEI layer and thereby form an interpenetrating architecture, which can reduce the Laplace pressure arising from the hydrophobic CNTs side and promote water transport. Together with the plentiful porous geometry, opposite wettability and interpenetrating network structure, this Janus membrane exhibited excellent screening performance for various dye molecules. With regard to CR, its permeance flux can reach up to 3110.2 ± 285 L $m^{-2}h^{-1}$ bar^{-1} with rejection efficiency about 98.8%, which is far beyond the majority of the separation membranes reported to date. Furthermore, this membrane showed excellent rejection performance for dye molecules even it was physical damage or chemical corrosion. This work may provide a new pathway to construct Janus materials to break the bottleneck between penetration and efficiency.

Declaration of Competing Interest

The authors declare that they have no known competing financial interests or personal relationships that could have appeared to influence the work reported in this paper.

Acknowledgements

We gratefully acknowledge the funding from the National Key Research and Development Program of China (2019YFC1606600, 2019YFC1606603), the Bureau of Frontier Science and Education of Chinese Academy of Sciences (QYZDB-SSW-SLH036), Special Fund for Basic Scientific Research of Central Colleges, Chang' an University (300102318403, 300102319306) and the K. C. Wong Education Foundation (GJTD-2019-13).

Appendix A. Supplementary data

Supplementary data to this article can be found online at https://doi.org/10.1016/j.cej.2020.127947.

References

[1] L. Nie, K. Goh, Y.u. Wang, J. Lee, Y. Huang, H.E. Karahan, K. Zhou, M.D. Guiver, T.-H. Bae, Realizing small-flake graphene oxide membranes for ultrafast size-dependent organic solvent nanofiltration, Sci. Adv. 6 (17) (2020) eaaz9184, https://doi.org/10.1126/sciadv.aaz9184.
[2] F. Soyekwo, C. Liu, H. Wen, Y. Hu, Construction of an electroneutral zinc incorporated polymer network nanocomposite membrane with enhanced selectivity for salt/dye separation, Chem. Eng. J. 380 (2020) 122560, https://doi.org/10.1016/j.cej.2019.122560.
[3] Z. Wang, Z. Wang, S. Lin, H. Jin, S. Gao, Y. Zhu, J. Jin, Nanoparticle-templated nanofiltration membranes for ultrahigh performance desalination, Nat. Commun. 9 (1) (2018), https://doi.org/10.1038/s41467-018-04467-3.
[4] Y. Song, R. Li, F. Pan, Z.e. He, H. Yang, Y. Li, L. Yang, M. Wang, H. Wang, Z. Jiang, Ultrapermeable graphene oxide membranes with tunable interlayer distances via vein-like supramolecular dendrimers, J. Mater. Chem. A 7 (31) (2019) 18642–18652, https://doi.org/10.1039/C9TA05909A.
[5] C. Kim, S. An, J. Lee, Q. Zeng, J.D. Fortner, Engineering graphene oxide laminate membranes for enhanced flux and boron treatment with polyethylenimine (PEI) polymers, ACS Appl. Mater. Interfaces 11 (1) (2019) 924–929, https://doi.org/10.1021/acsami.8b18545.s001.
[6] Y. Zhang, J. Ma, L.u. Shao, Ultra-thin trinity coating enabled by competitive reactions for unparalleled molecular separation, J. Mater. Chem. A 8 (10) (2020) 5078–5085, https://doi.org/10.1039/C9TA12670H.
[7] W. Wang, C. Xie, L. Zhu, B. Shan, C. Liu, F. Cui, A novel 3-dimensional graphene-based membrane with superior water flux and electrocatalytic properties for organic pollutant degradation, J. Mater. Chem. A 7 (1) (2019) 172–187, https://doi.org/10.1039/C8TA07976E.
[8] P. Zhang, J.-L. Gong, G.-M. Zeng, B. Song, W. Cao, H.-Y. Liu, S.-Y. Huan, P. Peng, Novel "loose" GO/MoS_2 composites membranes with enhanced permeability for effective salts and dyes rejection at low pressure, J. Membr. Sci. 574 (2019) 112–123, https://doi.org/10.1016/j.memsci.2018.12.046.
[9] Y. Kang, Y. Xia, H. Wang, X. Zhang, 2D Laminar membranes for selective water and ion transport, Adv. Funct. Mater. 29 (29) (2019) 1902014, https://doi.org/10.1002/adfm.201902014.
[10] L. Wang, M.S.H. Boutilier, P.R. Kidambi, D. Jang, N.G. Hadjiconstantinou, R. Karnik, Fundamental transport mechanisms, fabrication and potential applications of nanoporous atomically thin membranes, Nat. Nanotech 12 (6) (2017) 509–522, https://doi.org/10.1038/nnano.2017.72.
[11] X.L. Cui, X.L. Wu, J. Zhang, J.T. Wang, H.Q. Zhang, F.G. Du, L.B. Qu, X.Z. Cao, P. Zhang, A loosely stacked lamellar membrane by irregular Mo_S2 flakes for ultrahigh water and organics permeation, J. Mater. Chem. A 7 (2019) 12698–12705, https://doi.org/10.1039/C9TA03159F.
[12] L. Ries, E. Petit, T. Michel, C.C. Diogo, C. Gervais, C. Salameh, M. Bechelany, S. Balme, P. Miele, N. Onofrio, D. Voiry, Enhanced sieving from exfoliated MoS_2 membranes via covalent functionalization, Nat. Mater. 18 (10) (2019) 1112–1117, https://doi.org/10.1038/s41563-019-0464-7.
[13] H. Li, T.-J. Ko, M. Lee, H.-S. Chung, S.S. Han, K.H. Oh, A. Sadmani, H. Kang, Y. Jung, Experimental realization of few layer two-dimensional MoS 2 membranes of near atomic thickness for high efficiency water desalination, Nano Lett. 19 (8) (2019) 5194–5204, https://doi.org/10.1021/acs.nanolett.9b01577.s001.
[14] Z. Cao, V. Liu, A. Barati Farimani, Why is single-layer MoS 2 a more energy efficient membrane for water desalination? ACS Energy Lett. 5 (7) (2020) 2217–2222, https://doi.org/10.1021/acsenergylett.0c00923.s003.
[15] K. Dey, S.B.B. Kunjattu, A.M. Chahande, R. Banerjee, Nanoparticle size-fractionation through self-standing porous covalent and organic framework films, Angew. Chem. Int. Ed. 58 (2019) 1–6, https://doi.org/10.1002/anie.201813481.

[16] S. Kandambeth, B.P. Biswal, H.D. Chaudhari, K.C. Rout, S. Kunjattu, S. Mitra, S. Karak, A. Das, R. Mukherjee, U.K. Kharul, R. Banerjee, Selective molecular sieving in self-standing porous covalent-organic-framework membranes, Adv. Mater. 29 (2) (2017) 1603945, https://doi.org/10.1002/adma.201603945.

[17] F. Xu, M. Wei, X. Zhang, Y. Wang, Ion rejection in covalent organic frameworks: revealing the overlooked effect of in-pore transport, ACS Appl. Mater. Interfaces 11 (48) (2019) 45246–45255, https://doi.org/10.1021/acsami.9b18234.s001.

[18] M. Jian, R. Qiu, Y. Xia, J. Lu, Y. Chen, Q. Gu, R. Liu, C. Hu, J. Qu, H. Wang, X. Zhang, Ultrathin water-stable metal-organic framework membranes for ion separation, Sci. Adv. 6 (23) (2020) eaay3998, https://doi.org/10.1126/sciadv.aay3998.

[19] W. Li, P. Su, Z. Li, Z. Xu, F. Wang, H. Ou, J. Zhang, G. Zhang, E. Zeng, Ultrathin metal–organic framework membrane production by gel–vapour deposition, Nat. Commun. 8 (1) (2017), https://doi.org/10.1038/s41467-017-00544-1.

[20] S.-Y. Fang, P. Zhang, J.-L. Gong, L. Tang, G.-M. Zeng, B. Song, W.-C. Cao, J. Li, J. Ye, Construction of highly water-stable metal-organic framework UiO-66 thin-film composite membrane for dyes and antibiotics separation, Chem. Eng. J. 385 (2020) 123400, https://doi.org/10.1016/j.cej.2019.123400.

[21] G. Liu, J. Shen, Y. Ji, Q. Liu, G. Liu, J. Yang, W. Jin, Two-dimensional Ti 2 CT x MXene membranes with integrated and ordered nanochannels for efficient solvent dehydration, J. Mater. Chem. A 7 (19) (2019) 12095–12104, https://doi.org/10.1039/C9TA01507H.

[22] Y. Fan, L. Wei, X. Meng, W. Zhang, N. Yang, Y. Jin, X. Wang, M. Zhao, S. Liu, An unprecedented high-temperature-tolerance 2D laminar MXene membrane for ultrafast hydrogen sieving, J. Membrane Sci. 569 (2019) 117–123, https://doi.org/10.1016/j.memsci.2018.10.017.

[23] J. Ran, T. Pan, Y.Y. Wu, C.Q. Chu, P. Cui, P.P. Zhang, X.Y. Ai, C.F. Fu, Z.J. Yang, T. W. Xu, Acid spacers endowing g-C_3N_4 membranes with superior permeability and stability, Angew. Chem. Int. Ed. 58 (2019) 16463–16468, https://doi.org/10.1002/anie.201908786.

[24] Y. Wang, L. Li, Y. Wei, J. Xue, H. Chen, L. Ding, Jürgen Caro, H. Wang, Water transport with ultralow friction through partially exfoliated g-C3 N4 nanosheet membranes with self-supporting spacers, Angew. Chem. Int. Ed. 56 (31) (2017) 8974–8980, https://doi.org/10.1002/anie.201701288.

[25] B. Mi, Graphene oxide membranes for ionic and molecular sieving, Science 343 (6172) (2014) 740–742, https://doi.org/10.1126/science:1250247.

[26] G. Zhao, H. Zhu, Cation–π interactions in graphene-containing systems for water treatment and beyond, Adv. Mater. 32 (22) (2020) 1905756, https://doi.org/10.1002/adma.201905756.

[27] J.Y. Xia, P. Xiao, J.C. Gu, T.Y. Chen, C.H. Liu, L.K. Yan, T. Chen, Interfacial self-assembled GR/GO ultrathin membranes in large scale for molecular sieving, J. Mater. Chem. A 6 (2020), https://doi.org/10.1039/D0TA05337F, doi: 10.1039/D0TA05337F.

[28] H. Liu, H. Wang, X. Zhang, Facile fabrication of freestanding ultrathin reduced graphene oxide membranes for water purification, Adv. Mater. 27 (2) (2015) 249–254, https://doi.org/10.1002/adma.201404054.

[29] M. Zhang, Y. Mao, G. Liu, G. Liu, Y. Fan, W. Jin, Molecular bridges stabilize graphene oxide membranes in water, Angew. Chem. Int. Ed. 59 (4) (2020) 1689–1695, https://doi.org/10.1002/anie.201913010.

[30] Z. Tan, S. Chen, X. Peng, L. Zhang, C. Gao, Polyamide membranes with nanoscale turing structures for water purification, Science 360 (6388) (2018) 518–521, https://doi.org/10.1126/science:aar6308.

[31] J. Park, H. Joo, M. Noh, Y. Namkoong, S. Lee, K.H. Jung, H.R. Ahn, S. Kim, J.-C. Lee, J.H. Yoon, Y. Lee, Systematic structure control of ammonium iodide salts as feasible UCST-type forward osmosis draw solutes for the treatment of wastewater, J. Mater. Chem. A 6 (3) (2018) 1255–1265, https://doi.org/10.1039/C7TA09741G.

[32] S. Zhou, Z. Xiong, F. Liu, H. Lin, J. Wang, T. Li, Q. Han, Q. Fang, Novel Janus membrane with unprecedented osmosis transport performance, J. Mater. Chem. A 7 (2) (2019) 632–638, https://doi.org/10.1039/C8TA08541B.

[33] Y. Zhao, H. Wang, H. Zhou, T. Lin, Directional fluid transport in thin porous materials and its functional applications, Small 13 (4) (2017) 1601070, https://doi.org/10.1002/smll.201601070.

[34] Z. Wang, X. Yang, Z. Cheng, Y. Liu, L. Shao, L. Jiang, Simply realizing "water diode" Janus membranes for multifunctional smart applications, Mater. Horiz. 4 (4) (2017) 701–708, https://doi.org/10.1039/C7MH00216E.

[35] J. Ji, Q. Kang, Y. Zhou, Y. Feng, X. Chen, J. Yuan, W. Guo, Y. Wei, L. Jiang, Osmotic power generation with positively and negatively charged 2D nanofluidic membrane pairs, Adv. Funct. Mater. 27 (2) (2017) 1603623, https://doi.org/10.1002/adfm.201603623.

[36] J. Wang, Z. Yuan, X. Wu, Y. Li, J. Chen, Z. Jiang, Beetle-inspired assembly of heterostructured lamellar membranes with polymer cluster–patterned surface for enhanced molecular permeation, Adv. Funct. Mater. 29 (23) (2019) 1900819, https://doi.org/10.1002/adfm.201900819.

[37] J. Liu, D. Hua, Y. Zhang, S. Japip, T.-S. Chung, Precise molecular sieving architectures with janus pathways for both polar and nonpolar molecules, Adv. Mater. 30 (11) (2018) 1705933, https://doi.org/10.1002/adma.201705933.

[38] C.-M. Kim, S. Hong, R. Li, I.S. Kim, P. Wang, Janus graphene oxide-doped, lamellar composite membranes with strong aqueous stability, ACS Sustainable Chem. Eng. 7 (7) (2019) 7252–7259, https://doi.org/10.1021/acssuschemeng.9b00282.s001.

[39] H. Zhou, Z. Guo, Superwetting Janus membranes: focusing on unidirectional transport behaviors and multiple applications, J. Mater. Chem. A 7 (21) (2019) 12921–12950, https://doi.org/10.1039/C9TA02682G.

[40] H.-C. Yang, J. Hou, V. Chen, Z.-K. Xu, Janus membranes: exploring duality for advanced separation, Angew. Chem. Int. Ed. 55 (43) (2016) 13398–13407, https://doi.org/10.1002/anie.201601589.

[41] P. Xiao, J. Gu, C. Wan, S. Wang, J. He, J. Zhang, Y. Huang, S.-W. Kuo, T. Chen, Ultrafast formation of free-standing 2D carbon nanotube thin films through capillary force driving compression on an air/water interface, Chem. Mater. 28 (19) (2016) 7125–7133, https://doi.org/10.1021/acs.chemmater.6b03420.s004.

[42] J. He, P. Xiao, W. Lu, J. Shi, L. Zhang, Y. Liang, C. Pan, S.-W. Kuo, T. Chen, A Universal high accuracy wearable pulse monitoring system via high sensitivity and large linearity graphene pressure sensor, Nano Energy 59 (2019) 422–433, https://doi.org/10.1016/j.nanoen.2019.02.036.

[43] N. Bui, E.R. Meshot, S. Kim, J. Peña, P.W. Gibson, K.J. Wu, F. Fornasiero, Ultrabreathable and protective membranes with sub-5 nm carbon nanotube pores, Adv. Mater. 28 (28) (2016) 5871–5877, https://doi.org/10.1002/adma.201600740.

[44] H. Huang, H. Shi, P. Das, J. Qin, Y. Li, X. Wang, F. Su, P. Wen, S. Li, P. Lu, F. Liu, Y. Li, Y. Zhang, Y. Wang, Z. Wu, H. Cheng, The chemistry and promising applications of graphene and porous graphene materials, Adv. Funct. Mater. 30 (41) (2020) 1909035, https://doi.org/10.1002/adfm.201909035.

[45] Y. Xu, G. Peng, J. Liao, J. Shen, C. Gao, Preparation of molecular selective GO/$DTiO_2$-PDA-PEI composite nanofiltration membrane for highly pure dye separation, J. Membrane Sci. 601 (2020) 117727, https://doi.org/10.1016/j.memsci.2019.117727.

[46] L. Hou, Nü Wang, X. Man, Z. Cui, J. Wu, J. Liu, S. Li, Y. Gao, D. Li, L. Jiang, Y. Zhao, Interpenetrating janus membrane for high rectification ratio liquid unidirectional penetration, ACS Nano 13 (4) (2019) 4124–4132, https://doi.org/10.1021/acsnano.8b08753.s004.

[47] Q. Zhang, Y. Li, Y. Yan, X. Zhang, D. Tian, L. Jiang, Highly flexible monolayered porous membrane with superhydrophilicity–hydrophilicity for unidirectional liquid penetration, ACS Nano 14 (6) (2020) 7287–7296, https://doi.org/10.1021/acsnano.0c02558.s006.

[48] J. Xia, P. Xiao, J. Gu, T. Chen, C. Liu, L. Yan, T. Chen, Interfacial self-assembled GR/GO ultrathin membranes on a large scale for molecular sieving, J. Mater. Chem. A 8 (36) (2020) 18735–18744, https://doi.org/10.1039/D0TA05337F.

[49] J.J. Lu, Y.H. Gu, Y. Chen, X. Yan, Y.J. Guo, W.Z. Lang, Sep. Purif. Technol. 210 (2019) 737–745, https://doi.org/10.1016/j.seppur.2018.08.065.

[50] G. Liu, W. Jin, Graphene oxide membrane for molecular separation: challenges and opportunities, Sci. China Mater. 61 (8) (2018) 1021–1026, https://doi.org/10.1007/s40843-018-9276-8.

[51] C. Yin, Z. Zhang, J. Zhou, Y. Wang, Single-layered nanosheets of covalent triazine frameworks (CTFs) by mild oxidation for molecular-sieving membranes, ACS Appl. Mater. Interfaces 12 (16) (2020) 18944–18951, https://doi.org/10.1021/acsami.0c03246.s001.

[52] J. Wang, P. Zhang, B. Liang, Y. Liu, T. Xu, L. Wang, B. Cao, K. Pan, Graphene oxide as effective barrier on a porous nanofibrous membrane for water treatment, ACS Appl. Mater. Interfaces 8 (2016) 6211–6218, https://doi.org/10.1021/acsami.5b12723.

[53] X. Zhang, H. Li, J. Wang, D. Peng, J. Liu, Y. Zhang, In-situ grown covalent organic framework nanosheets on graphene for membrane-based dye/salt separation, J. Membrane Sci. 581 (2019) 321–330, https://doi.org/10.1016/j.memsci.2019.03.070.

[54] Q.Q. Yu, X.D. You, H. Wu, Y.L. Su, R.N. Zhang, Y.N. Liu, C. Yang, J.L. Shen, J. Q. Yuan, Z.Y. Jiang, Ultrathin fluorinated self-cleaning membranes via coordination driven metal-bridged assembly for water purification, J. Mater. Chem. A 8 (2020) 4505–4514, https://doi.org/10.1039/C9TA13957E.

[55] L. Wang, N. Wang, G. Zhang, S. Ji, Covalent crosslinked assembly of tubular ceramic-based multilayer nanofiltration membranes for dye desalination, AIChE J. 59 (10) (2013) 3834–3842, https://doi.org/10.1002/aic.14093.

[56] H. Fan, J. Gu, H. Meng, A. Knebel, J. Caro, High-flux membranes based on the covalent organic framework COF-LZU1 for selective dye separation by nanofiltration, Angew. Chem. Int. Ed. 57 (15) (2018) 4083–4087, https://doi.org/10.1002/anie.201712816.

[57] J. Yang, G.-S. Lin, C.-Y. Mou, K.-L. Tung, Mesoporous silica thin membrane with tunable pore size for ultrahigh permeation and precise molecular separation, ACS Appl. Mater. Interfaces 12 (6) (2020) 7459–7465, https://doi.org/10.1021/acsami.9b21042.s001.

[58] X.-N. Chen, L.-S. Wan, Q.-Y. Wu, S.-H. Zhi, Z.-K. Xu, Mineralized polyacrylonitrile-based ultrafiltration membranes with improved water flux and rejection towards dye, J. Membrane Sci. 441 (2013) 112–119, https://doi.org/10.1016/j.memsci.2013.02.054.

[59] L. Yang, Z. Wang, J. Zhang, Zeolite imidazolate framework hybrid nanofiltration (NF) membranes with enhanced permselectivity for dye removal, J. Membrane Sci. 532 (2017) 76–86, https://doi.org/10.1016/j.memsci.2017.03.014.

[60] C. Zhang, K. Wei, W. Zhang, Y. Bai, Y. Sun, J. Gu, Graphene oxide quantum dots incorporated into a thin film nanocomposite membrane with high flux and antifouling properties for low-pressure nanofiltration, ACS Appl. Mater. Interfaces 9 (12) (2017) 11082–11094, https://doi.org/10.1021/acsami.6b12826.s001.

[61] Q. Chen, P. Yu, W. Huang, S. Yu, M. Liu, C. Gao, High-flux composite hollow fiber nanofiltration membranes fabricated through layer-by-layer deposition of oppositely charged crosslinked polyelectrolytes for dye removal, J. Membrane Sci. 492 (2015) 312–321, https://doi.org/10.1016/j.memsci.2015.05.068.

[62] M. Liu, Q. Chen, K. Lu, W. Huang, Z. Lü, C. Zhou, S. Yu, C. Gao, High efficient removal of dyes from aqueous solution through nanofiltration using diethanolamine-modified polyamide thin-film composite membrane, Sep. Purif. Technol. 173 (2017) 135–143, https://doi.org/10.1016/j.seppur.2016.09.023.

[63] Y. Li, Y. Su, X. Zhao, X. He, R. Zhang, J. Zhao, X. Fan, Z. Jiang, Antifouling, high-flux nanofiltration membranes enabled by dual functional polydopamine, ACS Appl. Mater. Interfaces 6 (8) (2014) 5548–5557, https://doi.org/10.1021/am405990g.

[64] J. Zhu, A. Uliana, J. Wang, S. Yuan, J. Li, M. Tian, K. Simoens, A. Volodin, J. Lin, K. Bernaerts, Y. Zhang, B. Van der Bruggen, Elevated salt transport of antimicrobial loose nanofiltration membranes enabled by copper nanoparticles via fast bioinspired deposition, J. Mater. Chem. A 4 (34) (2016) 13211–13222, https://doi.org/10.1039/C6TA05661J.

[65] R. Bi, Q. Zhang, R. Zhang, Y. Su, Z. Jiang, Thin film nanocomposite membranes incorporated with graphene quantum dots for high flux and antifouling property, J. Membrane Sci. 553 (2018) 17–24, https://doi.org/10.1016/j.memsci.2018.02.010.

[66] C. Zhou, Y. Shi, C. Sun, S. Yu, M. Liu, C. Gao, Thin-film composite membranes formed by interfacial polymerization with natural material sericin and trimesoyl chloride for nanofiltration, J. Membrane Sci. 471 (2014) 381–391, https://doi.org/10.1016/j.memsci.2014.08.033.

[67] J. Jang, Y.T. Nam, D. Kim, Y.-J. Kim, D.W. Kim, H.-T. Jung, Turbostratic nanoporous carbon sheet membrane for ultrafast and selective nanofiltration in viscous green solvents, J. Mater. Chem. A 8 (17) (2020) 8292–8299, https://doi.org/10.1039/D0TA00804D.

[68] R. Wang, X. Shi, A. Xiao, W. Zhou, Y. Wang, Interfacial polymerization of covalent organic frameworks (COFs) on polymeric substrates for molecular separations, J. Membr. Sci. 566 (2018) 197–204, https://doi.org/10.1016/j.memsci.2018.08.044.

[69] G. Li, W. Wang, Q. Fang, F. Liu, Covalent triazine frameworks membrane with highly ordered skeleton nanopores for robust and precise molecule/ion separation, J. Membr. Sci. 595 (2020) 117525, https://doi.org/10.1016/j.memsci.2019.117525.

[70] N.A. Khan, J. Yuan, H. Wu, L. Cao, R. Zhang, Y. Liu, L. Li, A.U. Rahman, R. Kasher, Z. Jiang, Mixed nanosheet membranes assembled from chemically grafted graphene oxide and covalent organic frameworks for ultra-high water flux, ACS Appl. Mater. Interfaces 11 (32) (2019) 28978–28986, https://doi.org/10.1021/acsami.9b09945.s001.

[71] W. Yan, D. Miao, A.A. Babar, J. Zhao, Y. Jia, B. Ding, X. Wang, Multi-scaled interconnected inter- and intra-fiber porous janus membranes for enhanced directional moisture transport, J. Colloid Interface Sci. 565 (2020) 426–435, https://doi.org/10.1016/j.jcis.2020.01.063.

[72] H.-C. Yang, Y. Xie, J. Hou, A.K. Cheetham, V. Chen, S.B. Darling, Janus membranes: creating asymmetry for energy efficiency, Adv. Mater. 30 (43) (2018) 1801495, https://doi.org/10.1002/adma.201801495.

[73] X. Tian, H. Jin, J. Sainio, R.H.A. Ras, O. Ikkala, Droplet and fluid gating by biomimetic janus membranes, Adv. Funct. Mater. 24 (38) (2014) 6023–6028, https://doi.org/10.1002/adfm.201400714.

[74] R.K. Joshi, P. Carbone, F.C. Wang, V.G. Kravets, Y. Su, I.V. Grigorieva, H.A. Wu, A. K. Geim, R.R. Nair, Precise and ultrafast molecular sieving through graphene oxide membranes, Science 343 (6172) (2014) 752–754, https://doi.org/10.1126/science:1245711.

[75] C. Pei, Y. Peng, Y. Zhang, D. Tian, K. Liu, L. Jiang, An integrated Janus mesh: underwater bubble antibuoyancy unidirectional penetration, ACS Nano 12 (6) (2018) 5489–5494, https://doi.org/10.1021/acsnano.8b01001.s001.